Building and Environment 282 (2025) 113233

Contents lists available at ScienceDirect

Building and Environment

journal homepage: www.elsevier.com/locate/buildenv

The resilience paradox of rooftop PV: Building cooling penalties and heat risks

Liutao Chen [a], Shihong Zhang [a], Ip Cheng [a], Haoran Chang [b], Fei Chen [c], Mengying Li [b], Zhe Wang [a,*]

[a] Department of Civil and Environmental Engineering, Hong Kong University of Science and Technology, Hong Kong Special Administrative Region, China
[b] Department of Mechanical Engineering & Research Institute for Smart Energy, Hong Kong Polytechnic University, Hong Kong Special Administrative Region, China
[c] Division of Environment and Sustainability, Hong Kong University of Science and Technology, Hong Kong Special Administrative Region, China

ARTICLE INFO

Keywords:
Rooftop photovoltaic (PV)
Urban Heat Island (UHI)
Building cooling demands
Thermal comfort
Passive survivability

ABSTRACT

Rooftop photovoltaic (PV) systems reduce reliance on fossil fuels but may unintentionally exacerbate urban heat. This study investigates the competing thermal effects of rooftop PV –microclimate warming versus panel shading – through environmental monitoring and building energy simulations during July 2024 heatwaves in a humid subtropical climate.

Field measurements showed that PV installations elevated ambient temperatures by over 5 °C compared to conventional bare roof, creating localized “PV heat islands”. Energy simulations of top-floor spaces revealed that PV-induced warming fully offset shading benefits, resulting in a net 1.5 % increase in cooling energy demand. While generating 71 % of monthly electricity demand at 50 % coverage, PV-induced warming significantly increased occupants "Extreme Danger" heat exposure by 29.8 % during power outages.

This highlights a critical resilience paradox: while rooftop PV systems enhance energy sustainability, they may compromise thermal safety during extreme heat. These findings highlight the need for climate-adaptive PV designs that balance energy generation with urban heat mitigation, particularly in heat-vulnerable urban areas.

1. Introduction

The global transition toward renewable energy has led to widespread adoption of rooftop photovoltaic (PV) systems [1–4]. While these installations generate clean electricity, their dual function as energy generators and thermal modifiers in urban environments remains insufficiently understood [5–8], particularly their net effects on microclimates and building energy performance.

Existing research on PV climate effects has primarily employed two approaches: computational fluid dynamics (CFD) models for panel-to-neighbourhood scale analysis [8–11] and numerical meteorological models for neighbourhood-to-global scale assessments [12–21]. These studies report conflicting daytime temperature impacts during hot periods, ranging from cooling effects (−1.0 °C in Singapore [19], −0.7 °C in Phoenix [12] and Guangzhou [20]) to warming effects (+1.5 °C in Kolkata [18], +1.9 °C in Sydney [18]). While informative, these models face reliability challenges due to simplified assumptions and unvalidated parameterization schemes [7,22], highlighting the need for validation through field measurements.

Field studies at utility-scale PV plants have identified a localized PV heat island (PVHI) effect [23–25], with average daily maximum temperatures 1.3 °C higher than surrounding desert areas [24] and nighttime temperatures 3–4 °C warmer than wildlands [25]. However, urban environments may respond differently due to distinct surface properties and atmospheric conditions. The few available real-world scale urban measurement studies – limited by safety and regulatory constraints – consistently show PV systems create daytime warming (monthly average +0.75 °C [26] and +1.18 [22]) with slight nighttime cooling (monthly average −0.2 °C) [22,26,27]. These findings are critical for understanding microclimate impacts of rooftop PV deployment.

PV systems also provide significant shading benefits, reducing rooftop solar radiation and cooling loads [28–32]. Experimental data from Shaanxi, China demonstrate PV-shaded roofs can be 10 °C cooler at peak sunlight than exposed roofs [30], while measurements in Western Greece show temperature differences of 12.9 °C (summer) and 8.3 °C (winter) at noon, with around 2 °C nighttime cooling [31]. These

* Corresponding author.
E-mail address: cezhewang@ust.hk (Z. Wang).

https://doi.org/10.1016/j.buildenv.2025.113233
Received 2 April 2025; Received in revised form 10 May 2025; Accepted 27 May 2025
Available online 28 May 2025

thermal modifications yield 17.8 % cooling energy savings but increase heating demand by 6.7 %. Importantly, the observed cooling benefits may be counterbalanced by PV-induced warming effects, highlighting the need for comprehensive assessment of net energy impacts.

Notably, urban climates and building energy systems engage in a complex positive feedback cycle [33]. Rising temperatures increase cooling demand (up to 8.5 % per 1 °C [34]), while waste heat from air conditioning (A/C) further elevates urban temperatures — creating a self-reinforcing cycle that increased energy use by additional 10 % in Osaka, Japan [35]. Li et al. [33] projected that neglecting these climate-energy interactions may lead to 120 % underestimation of future cooling needs in global cities.

Rooftop PV systems interact with this feedback cycle through three distinct mechanisms operating at different scales:

1. **Building-scale shading effect**: Direct reduction of solar heat gain and cooling load on host buildings.
2. **Local-to-global warming effect**: PV-induced thermal accumulation can propagate through horizontal advection. At large deployment scales, these thermal effects may alter atmospheric patterns and influence global climate, subsequently impacting cooling demand.
3. **Regional-to-global scale energy substitution**: By displacing fossil fuel-based power generation, PV systems reduce both greenhouse gas emissions and waste heat from power plants — collectively mitigating global warming and its associated urban cooling demand escalation.

Current research has largely examined PV's shading and climate effects in isolation, creating knowledge gaps in understanding how these competing effects interact. Our study addresses this need through an integrated approach combining field measurements with building energy simulations, specifically focusing on three key aspects:

1. **Microclimate modulation**: Quantify microclimate impact of rooftop PV during extreme hot conditions and identify the underlying mechanisms.
2. **Net energy impact**: Examine the net influence of rooftop PV on building cooling loads, considering both shading benefits and potential ambient warming.
3. **Resilience performance**: Assess PV's influence on indoor thermal comfort and passive survivability during power outage events.

These investigations provide physics-based evidence to inform climate-resilient PV deployment strategies that simultaneously optimize energy yield and thermal mitigation potential. The paper is organized as follows: Section 2 describes methodology, Section 3 presents results, Section 4 discusses implications, Section 5 concludes with key findings, and Section 6 addresses limitations and future research directions.

2. Method

2.1. Site description

The study was conducted at the Hong Kong University of Science and Technology (HKUST) campus (22.338 °N, 114.264 °E) in Hong Kong SAR, a city located in Southeast China, which features a typical monsoon-influenced humid subtropical climate (Köppen climate classification: Cwa). The region is characterized by hot, humid summers and mild winters, with an annual mean temperature of 23.5 °C, relative humidity of 78 %, and a total rainfall of 2431.2 mm [36]. July represents the hottest month, with mean temperatures reaching 29.9 °C and relative humidity of 81 %.

We compared two adjacent rooftop sites (>200 m² each) on a six-story campus building located 300 m from the coastline (Fig. 1**a**). The control site consisted of an aged concrete-tiled roof — normally exhibiting higher albedo than black roofing but lower than reflective coatings — serving administrative functions (Fig. 1**b**). The experimental site featured a 50 %-coverage PV system installed above office spaces with comparable occupancy patterns (Fig. 1**c**; see **Table S1** for occupancy schedule details). The PV array comprised 66 N-type mono-crystalline panels (JINKO company: JKM415N-6RL3; Size: 1855 × 1029 × 30 mm) with 21.74 % conversion efficiency and −0.34 %/ °C temperature coefficient. PV panel's electrical parameters included 415 Wp maximum power (Pmax), 46.77 V open-circuit voltage (Voc), and 12.06 A short-circuit current (Isc). Panels were mounted 1 m above the roof at 12° tilt with alternating southwest and northeast orientations, connected to optimizers and inverters for 15-minute resolution power monitoring. The sites were separated by 90 m to minimize cross-interference from shading or anthropogenic heat.

The environmental monitoring systems were deployed at both sites (Fig. 1**d**), including sensors for air temperature, humidity, wind, surface temperature, and solar irradiance (Fig. 1**e**: instrument specifications). Thermocouples were installed to monitor surface temperatures at both sites: (1) on the backside of southwest-facing PV panels (azimuth: 240°), and (2) on adjacent concrete bases that represent bare roof thermal characteristics. Prior to deployment, all temperature and humidity sensors were calibrated in a constant temperature and humidity chamber to ensure measurement accuracy. The air temperature and humidity data collected at 1.8 m height formed the basis for microclimate impact assessment in subsequent analyses.

2.2. Study period

This study focused on July 2024, Hong Kong's hottest month, to evaluate rooftop PV performance under extreme summer conditions. Meteorological data from a nearby 10-m high ground-based weather station (located 1 km southeast of the campus; instrument specifications in Fig. 1**f**) revealed two distinct heatwave periods (Fig. 2**a**). Following World Meteorological Organization (WMO) criteria (daily maximum temperatures > 32 °C for ≥3 consecutive days), heatwaves occurred from July 3–15 and July 20–25, with 22 total days exceeding 32 °C. Daily air temperatures (Ta) ranged from 24.5–35.9 °C (mean: 28.9 °C), creating ideal conditions for assessing PV thermal impacts during peak cooling demand.

The subtropical climate showed characteristic humidity patterns (Fig. 2**b**), with nighttime relative humidity (RH) approaching saturation and daytime levels dropping to 60–85 %, yielding a monthly average of 87.2 %. Rainfall accumulation reached 326.9 mm, including intense precipitation events (July 27–28) that maintained 100 % RH. Solar irradiance exhibited strong diurnal variability (Fig. 2**c**), with higher radiation coinciding with elevated temperatures, while overcast or rainy days showed reduced irradiance intensity. Wind speeds averaged 2.3 m/s at 10-m height (Fig. 2**d**).

2.3. Research workflow and simulation scenario

The study combines field measurements with energy simulations to evaluate rooftop PV impacts. As illustrated in Fig. 3, the methodology comprises four main phases: (1) experiment data preprocessing and quality control, (2) microclimate impact analysis, (3) building energy impact assessment, and (4) passive survivability evaluation during power outages. Each phase is described in detail below.

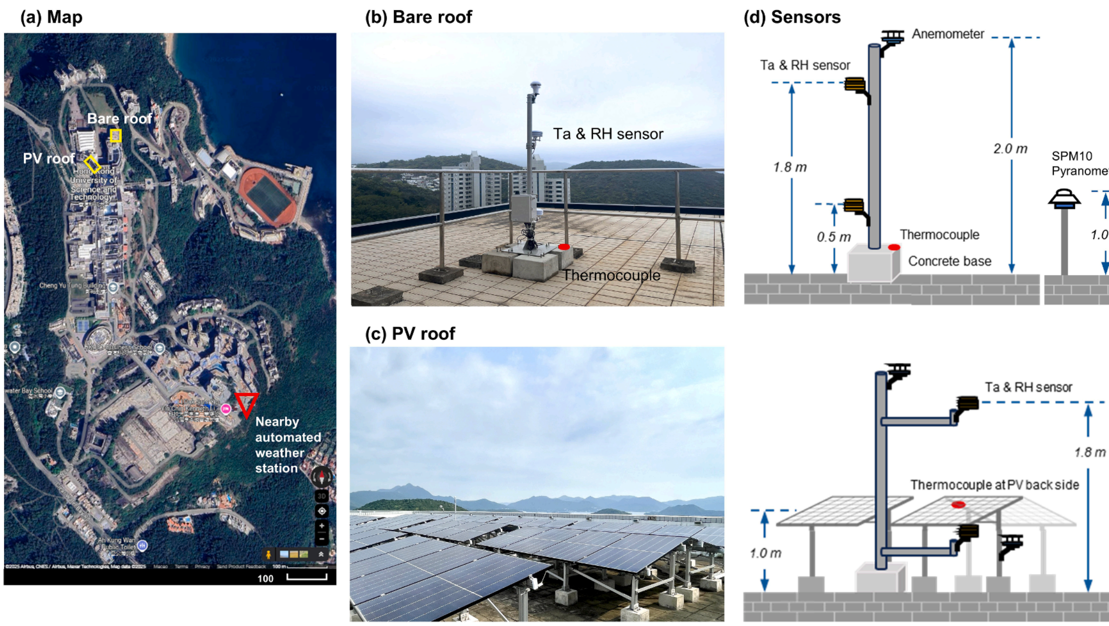

(e) Technical specifications of rooftop measurement instruments

Device name	Legend	Variables	Range	Resolution	Accuracy
QTHPB Air temperature & relative humidity sensor		Air temperature (Ta)	-40 to +60 ℃	0.1 °C	± 0.5 °C
		Relative humidity (RH)	0 – 100 %	0.5 %	± 3 %
HY-SA3E Ultrasonic anemometer		Wind Speed	0 – 70 m/s	0.1 m/s	± 3 %
		Wind Direction	0 – 359°	1°	± 3°
K-type Thermocouple		Surface temperature	-189 to +660 ℃	0.1 °C	± 0.5 °C
SMP10 Pyranometer		Global horizontal irradiance	0 to 1600 W/m²	0.1 W/m²	< ±7 W/m² (at 200 W/m²)

(f) Technical specifications of 10-m automatic weather station

Device name	Variables	Range	Resolution	Accuracy
Cambell Scientific HMP60-L Air temperature & relative humidity sensor	Air temperature (Ta)	-40 to +60 ℃	Not given	± 0.6 °C
	Relative humidity (RH)	0 – 100 %	Not given	± 3 % (0 – 90 % RH); ± 5 % (90 – 100 % RH)
Young MODEL 85000 Anemometer	Wind Speed	0 – 70 m/s	0.1 m/s	± 2 % or 0.1 m/s
	Wind Direction	0 – 360°	1°	± 2°
Cambell Scientific TE525-L Rain Guage	Rainfall	Not given	1 tip (4.73 ml/tip)	Uncertainty: 1.0% up to 50 mm/h (2 in./h)
LI-COR LI-200R Pyranometer	Global horizontal irradiance	0 to 3000 W/m²	Not given	±3% typical; ±5% maximum

Fig. 1. Study site and environmental monitoring system. (a) Geographical location of the study site, (b) Conventional bare roof, (c) PV roof, (d) Schematic diagram of sensor deployment. Detailed technical specifications of (e) rooftop measurement instruments and (f) the 10-m automatic weather station.

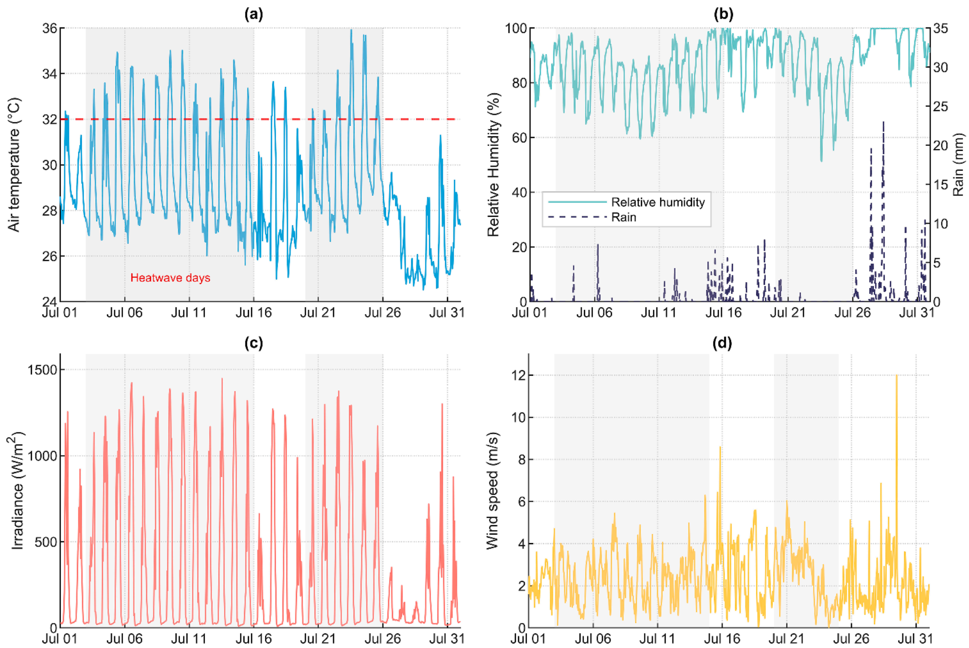

Fig. 2. Meteorological conditions in July 2024. (a) Air temperature (°C), (b) Relative humidity and Rainfall (mm), (c) Global horizontal irradiance (W/m^2), and (d) Wind speed (m/s). Heatwave periods are shaded in grey colour. Data from nearby automatic weather station.

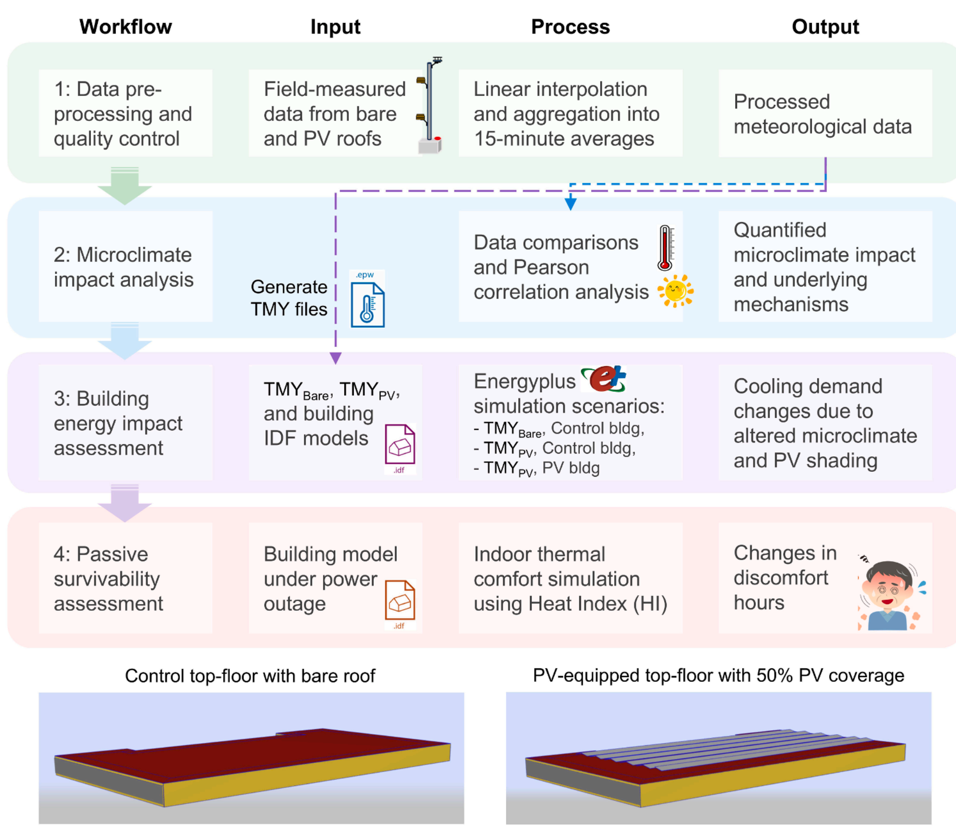

Fig. 3. Four-phase research workflow. (1) Data processing, (2) Microclimate analysis, (3) Energy simulation, and (4) Resilience assessment.

2.3.1. *Experiment data preprocessing and quality control*

Meteorological field measurement data were collected at 1-minute intervals, achieving high data completeness (98 % for bare roof, 92 % for PV roof). Most missing data (80 %) consisted of single-minute gaps, attributed to transient signal transmission issues. To address these gaps and maintain meaningful temporal patterns, the raw 1-minute data was linearly interpolated and then aggregated into 15-minute averages. This 15-minute interval was chosen as it aligns with typical maintenance schedules for rooftop equipment, ensuring that the average data reflect realistic operational conditions while minimizing the impact of transient anomalies.

2.3.2. Microclimate impact analysis

The processed 15-minute data from both roof configurations – including air temperature, humidity, solar irradiance, and surface temperatures – were analysed using MATLAB R2024a for data processing and visualization. Statistical analysis employed Pearson correlation coefficients to evaluate variable relationships, with all reported correlations accompanied by p-values to establish statistical significance ($\alpha = 0.05$ threshold). This analysis aims to quantify the localized thermal effects of rooftop PV under various meteorological conditions during July. The complete microclimate analysis results, including correlation matrices, statistical significance testing outcomes, 95 % confidence intervals, and MATLAB-generated visualizations, are presented in Section 3.1.

2.3.3. Building energy impact assessment

The energy performance assessment employed EnergyPlus v23.2 to simulate and evaluate two competing effects of rooftop PV systems: microclimate modification and shading impacts on building cooling demand. To accurately represent localized microclimate conditions, we developed customized weather files by replacing standard Typical Meteorological Year (TMY) data with site-specific meteorological measurements. Hourly averages of air temperature, relative humidity, and solar irradiance from both the bare roof and PV roof sites were incorporated into modified TMY_{Bare} and TMY_{PV} files, with original TMY values retained for any missing measurements to ensure data continuity.

Three distinct simulation scenarios were established to isolate different thermal effects, as summarized in Table 1. The Baseline Scenario A employed TMY_{Bare} with a conventional bare roof configuration. Scenario B applied TMY_{PV} data while maintaining the same bare roof configuration, allowing isolation of microclimate effects (detailed in Section 3.2). Scenario C incorporated both the PV roof system and TMY_{PV} data to assess combined impacts. Cooling demand differences between these scenarios (B-A for microclimate effects, C-B for shading effects, and C-A for total impact) provided quantitative measures of PV system influences on cooling demand.

The simulation specifically focused on the top-floor office spaces (2317.5 m^2) based on three key considerations. **First**, field instrumentation at rooftop level captured microclimate modifications most relevant to adjacent spaces. **Second**, top-floor environments experience the most direct shading impacts from rooftop conditions. **Third**, whole-building simulations would require unverified assumptions about vertical thermal gradients, potentially introducing uncertainty.

The PV system was geometrically represented in EnergyPlus using *Shading:Building:Detailed* objects with dimensions matching field measurements (Fig. 1**c**), including 50 % PV coverage, 1.0 m panel separation height, and 12° tilt angle. This model accounted for critical thermal processes: solar radiation blockage, longwave radiative exchange between PV panels and roof surfaces, and convective heat transfer through EnergyPlus' surface heat balance algorithms. Electrical output was calculated using the *PhotovoltaicPerformance:Simple* model:

$$Power = A_{cell} \times G_T \times \eta_{eff} \times \eta_{invert},$$

where A_{cell} represents active solar cell area (m^2), G_T is total incident radiation (W/m^2), η_{eff} denotes module conversion efficiency (= 21.74 %), and η_{invert} is inverter efficiency (= 95 %).

In this study, "sensible cooling energy" refers to the energy required to lower indoor air temperature, and "latent cooling energy" refers to the energy required to remove moisture from the air. Both are supplied by the A/C system to the building for the timestep reported. The cooling electricity is calculated as the total cooling energy divided by the Coefficient of Performance (COP = 3.5). This comprehensive methodology provides a robust framework for quantifying the competing thermal effects of rooftop PV systems on building cooling demands under realistic operating conditions.

2.3.4. Passive survivability assessment

Passive survivability refers to a building's ability to maintain safe indoor conditions during extended power outages. To evaluate the impact of rooftop PV installations on this critical resilience metric, we conducted thermal comfort analysis using the heat index (HI) during power outage scenarios. HI combines air temperature and relative humidity to better represent human thermal perception than air temperature alone [37]. This approach is particularly relevant for Hong Kong's humid climate, where elevated humidity levels exacerbate discomfort by hindering the body's natural cooling mechanisms through perspiration.

The calculation of HI is based on the formula [38,39]:

$$\begin{aligned} HI = & -42.379 + 2.04901523T + 10.14333127R - 0.22475541TR \\ & - 0.00683783T^2 - 0.05481717R^2 + 0.00122874T^2R \\ & + 0.00085282TR^2 - 0.00000199T^2R^2. \end{aligned}$$

Where *HI* is heat index and *T* is air temperature, both in degrees Fahrenheit. *R* is relative humidity expressed as a percentage.

Simulations examined the same top-floor under complete power outage conditions (i.e., without any electricity consumption, including A/C) to quantify changes in indoor discomfort hours. HI effects on human health are categorized into five risk categories (Table 2): Safe, Caution, Extreme Caution, Danger, and Extreme Danger. This analysis provides critical insights into how rooftop PV installations may influence building resilience during extreme heat events when grid power is unavailable.

3. Results

3.1. Microclimate impact of rooftop PV: experimental evidence

Field measurements demonstrate statistically thermal modifications caused by the rooftop PV installation (Fig. 4). Compared to the bare roof (Fig. 4**a** and 4**c**), PV coverage consistently elevated daytime (6 AM to 5 PM) air temperatures by 0.67±0.82 °C (monthly mean ± standard

Table 2
Health risk categories based on Heat Index (HI) values [39].

Heat Index in Celsius	Heat Index Level
Less than 26.7 °C	**Safe**: no risk of heat hazard
26.7 °C - 32.2 °C	**Caution**: fatigue is possible with prolonged exposure and activity. Continuing activity could result in heat cramps.
32.2 °C - 39.4 °C	**Extreme caution**: heat cramps and heat exhaustion are possible. Continuing activity could result in heat stroke.
39.4 °C - 51.7 °C	**Danger**: heat cramps and heat exhaustion are likely; heat stroke is probable with continued activity.
over 51.7 °C	**Extreme danger**: heat stroke is imminent.

Table 1
Designed simulation scenarios to investigate the impact of altered microclimate and PV shading on building cooling demand after installing rooftops PV.

Scenario	Meteorological data	Building setting	Notes
A	Bare roof TMY_{Bare}	Control top-floor (with bare roof)	B – A: Impact of altered microclimate
B	PV roof TMY_{PV}	Control top-floor	C – B: Impact of PV shading effect
C	PV roof TMY_{PV}	PV-equipped top-floor	C – A: Total impact of microclimate and shading

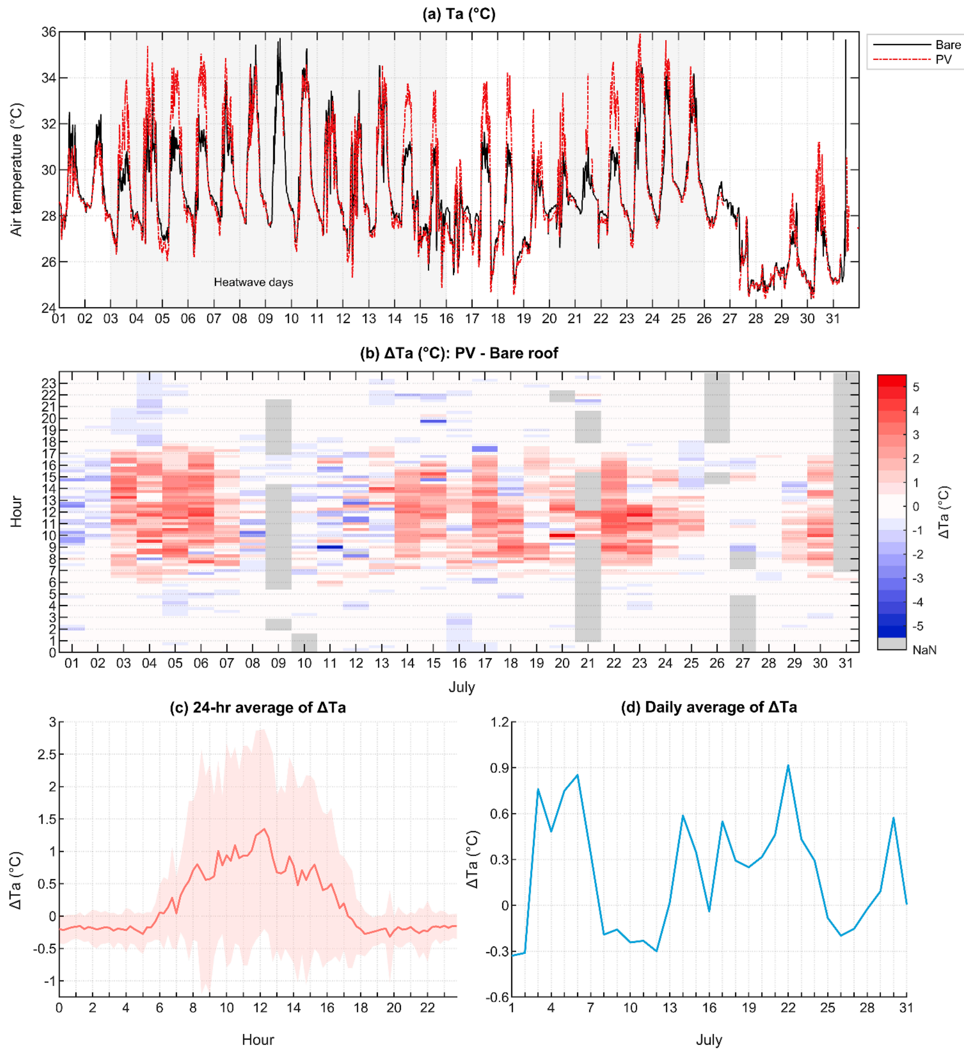

Fig. 4. Microclimate temperature variations at 15-minute resolution induced by rooftop PV installation during July 2024. (a) Diurnal air temperature (Ta) profiles at PV and bare roof sites, with grey shading indicating heatwave periods. (b) 15-minute interval temperature difference (ΔTa) between PV roof and bare roof throughout the study period. (c) Mean temperature difference aggregated from 15-minute data (solid line) with pink shading showing ±1 standard deviation. (d) Daily averaged temperature difference derived from 24-hour measurements.

deviation; 95 % confidence interval CI [0.38, 0.96]; $p < 0.001$), with peak warming occurring during midday hours. The warming effect intensified during heatwave events, reaching maximum observed differences of 5.2 °C at 10 AM on July 20 and 4.5 °C at 12 PM on July 23 (Fig. 4**b**). While occasional daytime cooling (1–2 °C) occurred on July 1–2, noon temperature measurements (12 PM) showed particularly strong warming, averaging 1.29±1.58 °C higher (95 % CI [0.74, 1.85]; $p < 0.001$) (Fig. 4**c**).

In contrast, nighttime measurements (6 PM – 5 AM) revealed a slight cooling effect, with PV roof reducing ambient temperatures by 0.20 ±0.13 °C (95 % CI [−0.25, −0.16]; $p < 0.001$). Daily aggregate temperature impacts peaked at +0.8 °C during extreme heat events (July 6 and 22; Fig. 4**d**), demonstrating PV systems' potential to intensify urban heating when cooling demand is highest. These findings highlight an important energy-environment trade-off: while rooftop PV installations generate renewable energy, they may exacerbate local warming during periods of peak thermal stress. The statistically robust daytime warming coupled with weaker nighttime cooling ($p < 0.001$) suggests complex microclimate interactions that warrant consideration in urban heat island mitigation strategies.

The observed warming patterns confirm previously reported mechanisms [7], where convective heat transfer from heated PV surfaces creates significant surface-atmosphere temperature gradients. During heatwave conditions (Fig. 5**a**), PV surface temperature (TPV) exhibited rapid morning increases, peaking at noon (reaching 65.8 °C on July 6) and remaining higher than bare roof surface temperatures (TR) until approximately 4 PM. The monthly analysis revealed an average noontime temperature differential (TPV-TR) of 9.66±6.86 °C (95 % CI [7.24, 12.07]; $p < 0.001$), with peak daily differences reaching 24.6 °C. This pronounced heating results from the combined effects of PV materials' high solar absorptivity, low thermal inertia, and decreased conversion efficiency during hot and sunny conditions, which collectively increase sensible heat release [22].

The surface heating patterns directly affected near-surface air temperatures through convective transfer. Fig. 5**b** reveals a strong positive correlation between surface (TPV - TR) and air temperature differences (ΔTa) during daylight hours, with correlation strength increasing at higher irradiance levels ($r = 0.79$ for irradiance > 1000 W/m^2, $p < 0.001$). Notably, while solar irradiance showed only moderate direct correlation with ΔTa ($r = 0.38$, $p < 0.001$), its primary influence occurred through PV surface heating (results not shown here), explaining the enhanced daytime warming observed during clear-sky conditions.

During evening transition, PV surfaces cooled rapidly, falling below conventional roof temperatures after 5 PM. Nighttime measurements showed PV panels maintained consistently lower temperatures than

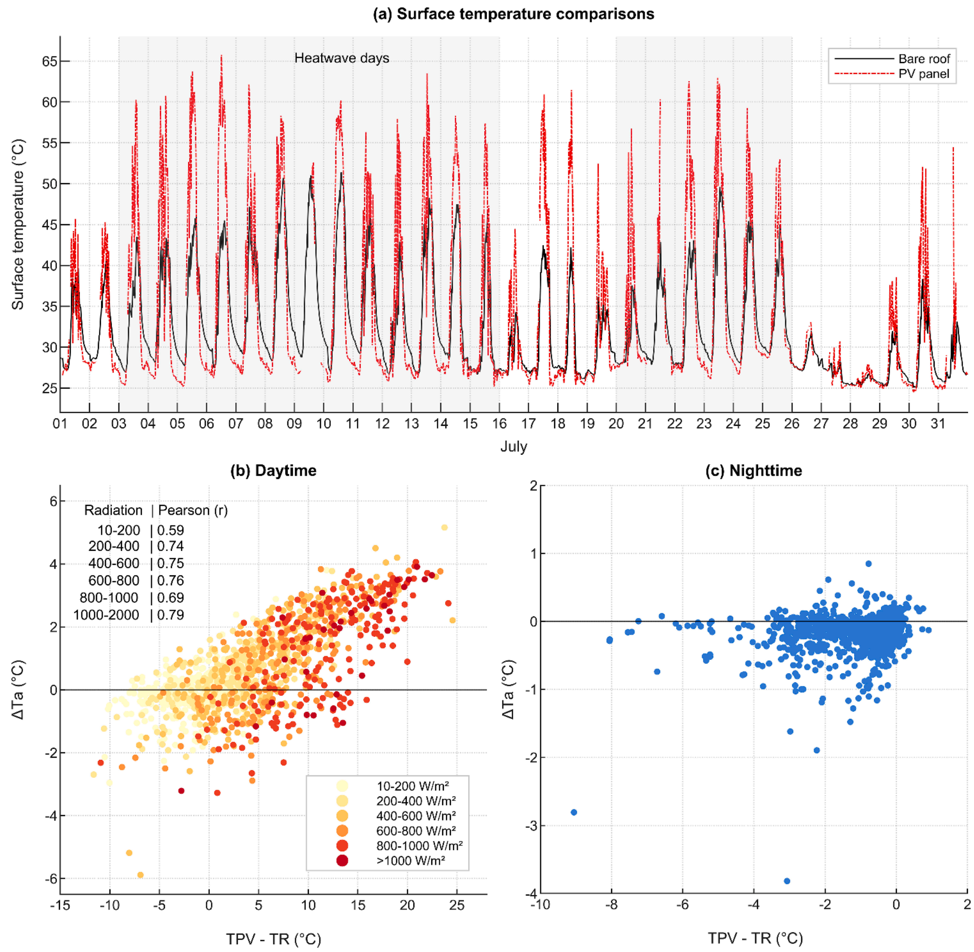

Fig. 5. Surface temperature dynamics and correlations at 15-minute resolution. (a) Temperature profiles of PV panel (TPV) versus concrete bare roof (TR). (b) Daytime and (c) nighttime correlations between surface temperature difference (TPV – TR) and air temperature differential (ΔTa).

concrete roof (mean difference: -1.84 ± 1.31 °C; 95 % CI: [-2.30, -1.38]; $p < 0.001$), with corresponding air temperature differences (ΔTa) predominantly clustered within -1 °C (Fig. 5**c**). The weak surface-air temperature correlation ($r = 0.16$, $p < 0.001$) during nighttime hours reflects minimal thermal influence from PV systems after sunset, as concrete roof gradually release stored heat while PV panels cool more rapidly [32].

Fig. 6 illustrates the diurnal relative humidity (RH) patterns observed at both rooftop sites. Throughout July (Fig. 6**a**), both sites exhibited persistent near-saturation conditions (RH ≈ 100 %), with only

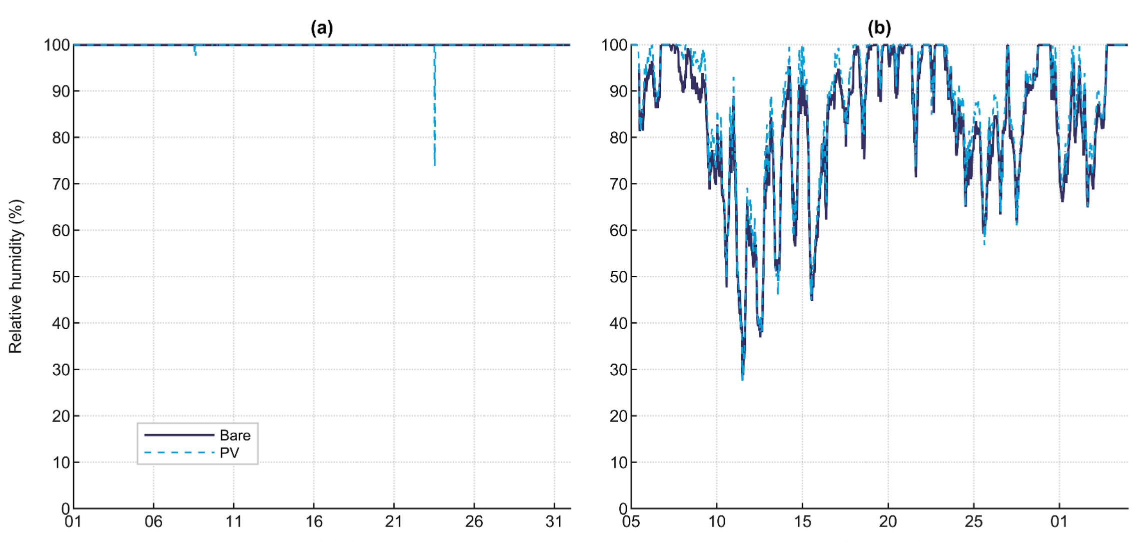

Fig. 6. Relative humidity comparisons between PV roof and bare roof. (a) July, and (b) February 2024.

two exceptions occurring on July 8 (3 PM) and July 23 (1 PM). These consistently high humidity levels result from the sites' coastal proximity (300 m from shore), where continuous moisture advection maintains saturation even during daytime heating periods. Accounting for the RH sensors' ±3 % accuracy, the 100 % readings correspond to actual humidity levels between 97–100 %, confirming the air was indeed near saturation. This pattern was consistently recorded by five additional rooftop sensors across campus, verifying that these observations reflect true regional atmospheric conditions rather than sensor errors.

To further demonstrate the proximity and comparability of these two sites, we analysed the temporal variations in RH during February (Fig. 6**b**), a winter month characterized by cooler air and reduced solar irradiance. The winter comparison reveals highly similar RH patterns between sites. The PV roof site showed slightly higher average RH (86.3 % versus 83.7 % at the bare roof), particularly during nighttime hours when cooler PV site enhanced near-surface moisture condensation. This seasonal analysis confirms that while PV installations can modify local humidity, their influence remains secondary to regional climatic drivers in coastal environments.

These findings have important implications for building cooling demand in coastal regions. While both roofs maintained near-saturation RH conditions during summer, the PV site's elevated ambient temperatures (Section 3.1) would correspond to higher absolute humidity levels. Our EnergyPlus simulations in Sections 3.2 demonstrate how this thermal-humidity interaction affects both sensible and latent cooling components. The dynamics differ fundamentally in inland environments where absolute humidity remains more stable. In such conditions, PV-induced warming would primarily influence sensible loads while potentially decreasing RH and latent loads – a fundamentally different dynamic we discussed through comparative modelling in Section 4.

3.2. Building energy impact due to ambient warming

Rooftop PV installations alter local microclimates, subsequently affecting building cooling demands. We quantified these effects through EnergyPlus simulations comparing top-floor office spaces under two meteorological conditions: Baseline (TMY_{Bare}) and PV-modified (TMY_{PV}) climates.

The analysis reveals distinct temporal patterns in cooling energy demand (Fig. 7). Sensible cooling requirements begin to rise at 7 AM, peak near midday, and decline to zero after 10 PM (Fig. 7**a**). During heatwave conditions, PV-induced warming amplifies peak sensible cooling demand by up to 11 %, with the most pronounced effects observed on July 6. The 24-hour average profile reveals that sensible cooling energy peaks at 1 PM, with PV-modified microclimate conditions increasing energy demand by 4.23 % on average ($p < 0.001$; Fig. 7**c**).

Notably, latent cooling energy demonstrates similar magnitude to

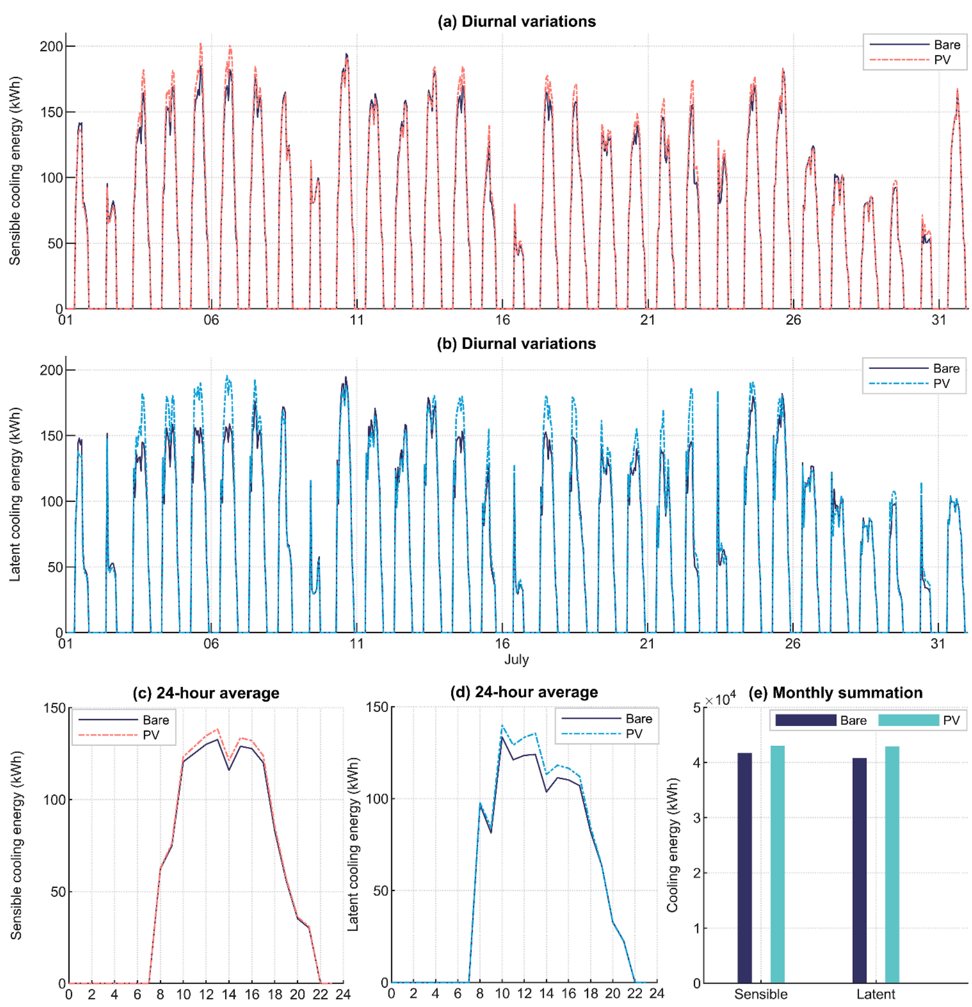

Fig. 7. Comparison of cooling energy demand in an office top-floor under bare roof and PV roof microclimate conditions. Diurnal variations of (a) sensible cooling energy (kWh) and (b) latent cooling energy (kWh). (c) and (d) 24-hour average diurnal patterns of sensible and latent cooling energy, respectively. (e) Monthly summation of sensible and latent cooling energy for Scenario A (Control top-floor, TMY_{Bare}) and Scenario B (Control top-floor, TMY_{PV}).

sensible cooling due to the building's substantial dehumidification requirements in the near-saturated environment (Fig. 7**b**). Although RH levels remained comparable between sites, warmer air temperatures at the PV site during midday increased the air's moisture-holding capacity, elevating absolute humidity. This thermal-hygric coupling effect substantially increased latent cooling requirements, with peak demand reaching 29 % higher than the control case at 1 PM on July 22 (Fig. 7**b**). The 24-hour average profile shows latent cooling peaking at 139.8 kWh by 10 AM and remaining 8.3 % higher on average during midday hours ($p < 0.001$; Fig. 7**d**).

Aggregated over the entire July study period, PV-induced microclimate changes increased sensible and latent cooling energy by 3.1 % and 5.3 %, respectively (Fig. 7**e, Table S2**). These findings highlight the critical need to account for microclimate- induced energy penalties when assessing rooftop PV systems, especially in humid coastal regions where dehumidification requirements are substantial.

3.3. Building energy impact due to PV shading

Rooftop PV systems substantially alter the thermal performance of underlying roof surfaces through their shading effects, with important implications for building cooling demands. We compared two roof configurations: (1) fully exposed bare roof and (2) roof with 50 % PV coverage, where surface temperatures represent area-weighted averages of shaded and exposed portions.

Our simulation reveals that PV shading significantly reduces underlying concrete roof surface temperatures, with maximum cooling of 13.4 °C observed at 2 PM on July 23 compared to exposed bare roof (Fig. 8**a**). The mean diurnal cycles illustrate that unshaded bare roof experiences rapid daytime heating from 6 AM, peaks at 45.9 °C by 1 PM, and stabilizes around 25 °C at night through radiative cooling (Fig. 8**b**). In contrast, PV-shaded roof shows more moderate temperature variations, with maximum daytime temperatures 7.2 °C lower (38.8 °C at 1 PM), and nighttime temperatures 1.1 °C higher ($p < 0.001$), as PV panels impede nocturnal heat loss and facilitate heat retention beneath them.

These surface temperature modifications directly impact building cooling requirements. The reduced daytime heat transfer through shaded roof yields substantial sensible cooling energy savings, exceeding 14 % at noon on July 23 (**Fig. S1**). Daily averages show PV shading reduces peak sensible cooling energy by 6.7 % ($p < 0.001$) during the 12–2 PM period (Fig. 8**c**). While latent cooling savings are minimal, peaking at just 2.3 % ($p < 0.001$; Fig. 8**d**), this finding demonstrates that PV shading primarily influences sensible rather than latent cooling components. Monthly aggregates indicate that PV shading provides overall reductions of 4.5 % in sensible cooling energy and 0.8 % in latent cooling energy (Fig. 8**e, Table S2**).

3.4. Total energy impact of rooftop PV on top-floor spaces

The above analyses demonstrate two competing thermal effects from rooftop PV installations: microclimate alterations that increase cooling energy demands (Section 3.2) versus shading effects that provide energy savings (Section 3.3). To evaluate the net impact, we conducted comparative simulations focusing on top-floor spaces with different usage patterns: office (daytime-dominated) and residential (nighttime-dominated) configurations. Key results are summarized in Table 3.

For office space, the net effect of PV installation shows a complex temporal pattern (Fig. 9**a**). During peak daytime hours, sensible cooling

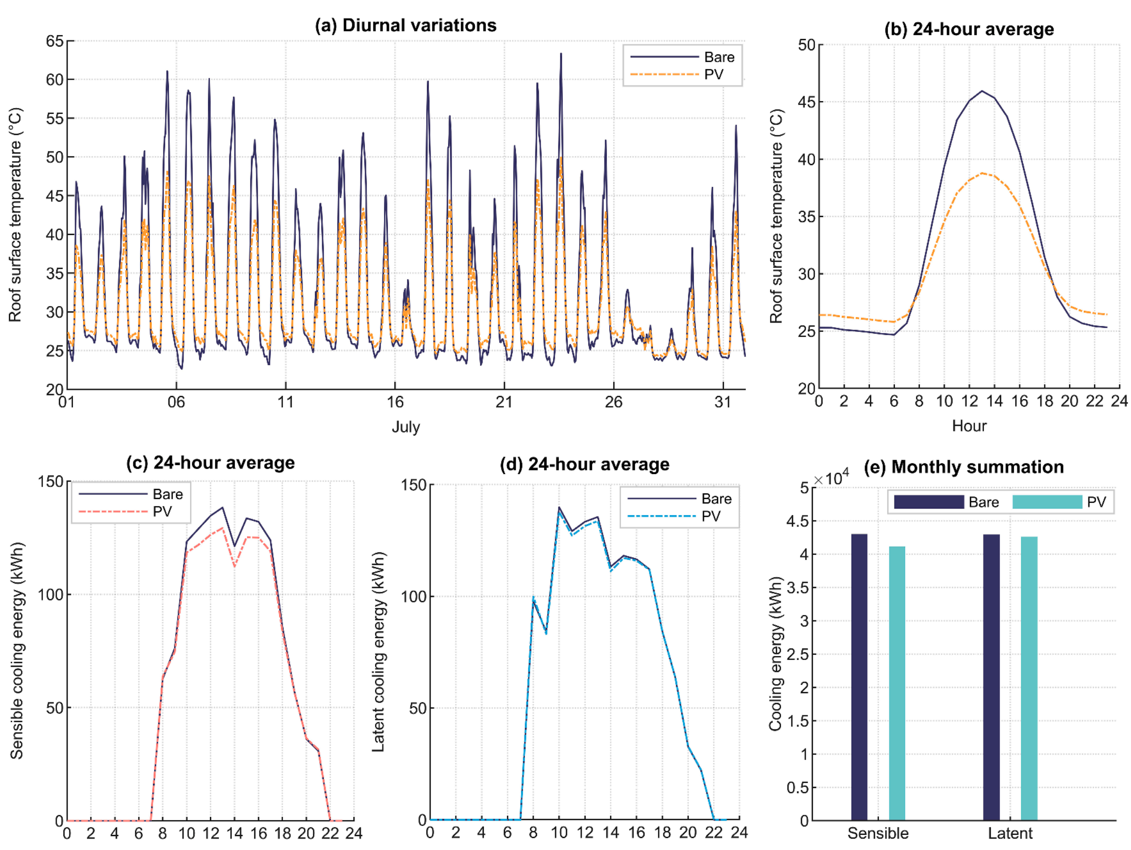

Fig. 8. Comparison of cooling energy influenced by PV shading. (a) Diurnal roof surface temperature comparison between fully exposed bare roof and PV-covered roof (area-weighted average of shaded and exposed sections). **(b)** 24-hour average diurnal temperature profiles. **(c)** and **(d)** 24-hour average diurnal variations of sensible and latent cooling energy, respectively. **(e)** Monthly summation of sensible and latent cooling energy for Scenario B (Control top-floor, TMY_{PV}) and Scenario C (PV-equipped top-floor, TMY_{PV}).

Table 3
Summary of monthly cumulative changes in cooling energy (kWh) due to microclimate and shading impacts of PV installations.

Impact on cooling energy	Sensible	Latent	Total
Office setting			
Microclimate impact	+1295.1 (+3.1 %)	+2159.8 (+5.3 %)	+3454.9 (+4.2 %)
Shading impact	−1881.5 (−4.5 %)	−315.6 (−0.8 %)	−2197.0 (−2.7 %)
Total	**−586.4 (−1.4 %)**	**+1844.3 (+4.5 %)**	**+1257.8 (+1.5 %)**
Residential setting			
Microclimate impact	+951.0 (+2.2 %)	+720.2 (+2.1 %)	+1671.2 (+2.1 %)
Shading impact	−1059.1 (−2.4 %)	−154.4 (−0.4 %)	−1213.5 (−1.5 %)
Total	**−108.1 (−0.2 %)**	**+ 565.8 (+1.6 %)**	**+457.7 (+0.6 %)**

energy demonstrates net savings of up to 3.8 kWh (3.0 % reduction) at 12 PM and 3 PM, **indicating shading effects outweigh local warming impacts**. However, post-6 PM conditions reveal increased sensible cooling energy as the PV canopy's heat retention elevates roof surface temperatures (Figs. 8**a** and 8**b**), enhancing nighttime heat conduction. This phenomenon is more pronounced in residential setting (Fig. 9**b**), where **despite minor ambient cooling, the trapped heat beneath PV panels dominates**, resulting in up to 2.3 % increase in sensible cooling demand at midnight.

Regarding latent cooling energy, there is a significant increase of up to 9.6 kWh at 1 PM for office spaces (Fig. 9**c**), representing an additional 7.8 % compared to the control case. This suggests that the **climate-induced humidity effects outweigh any shading benefits**. For residential spaces (Fig. 9**d**), latent cooling energy increases by up to 6.9 % at 1 PM, with minimal savings at night, peaking at merely 0.9 %. These findings demonstrate that while PV shading may moderate sensible cooling loads during peak hours, its influence on humidity-driven

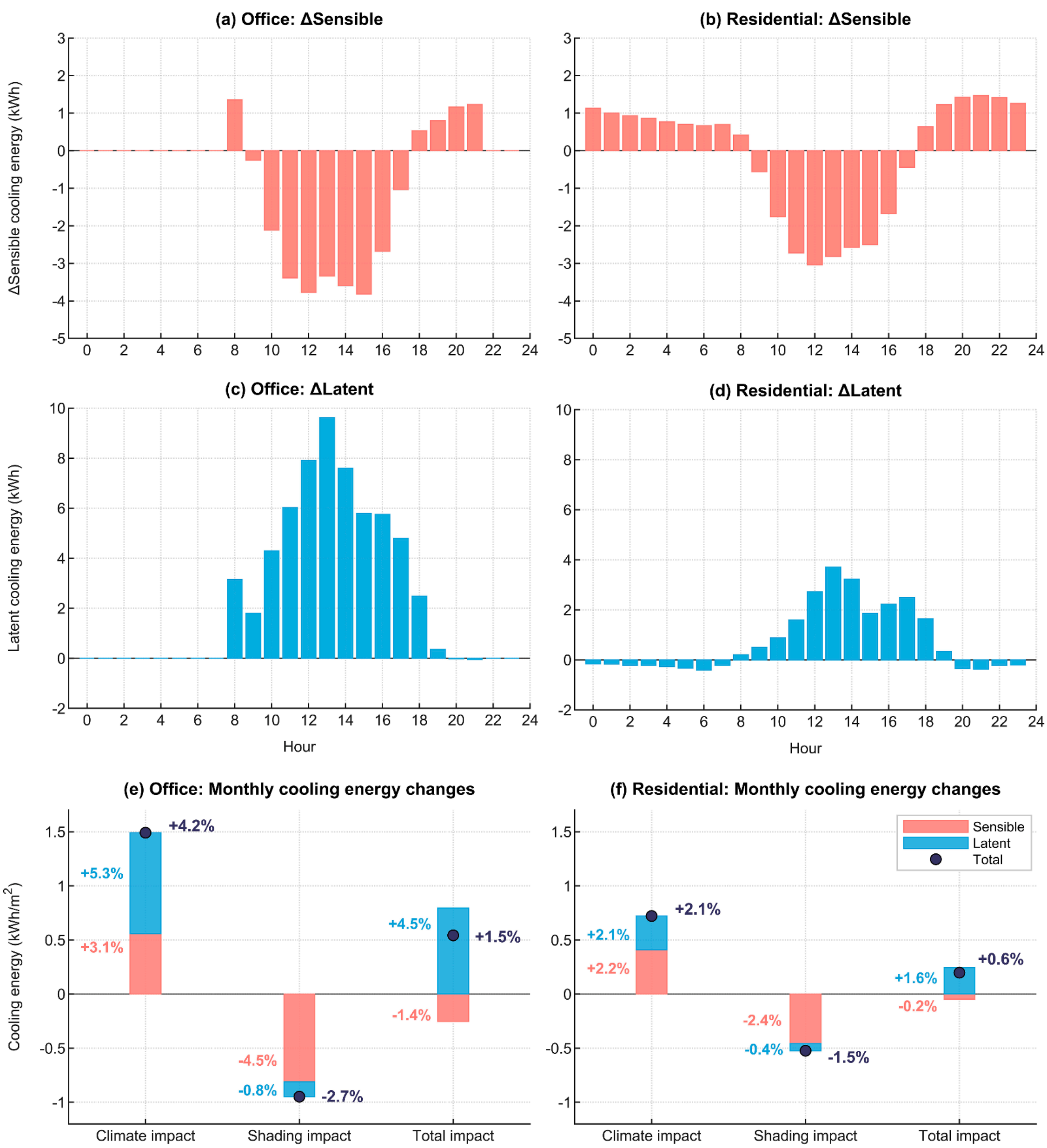

Fig. 9. Comparison of cooling energy differences between PV-equipped and control top-floor spaces. Diurnal average sensible cooling energy profile for (a) office and (b) residential use. Diurnal average latent cooling energy profile for (c) office and (d) residential use. Monthly cumulative cooling energy changes per floor area of different impacts for (e) office and (f) residential configurations.

cooling demands is consistently negative.

The analysis reveals significant temporal variations in cooling energy demands across different space types (**Figs. S2** and **S3**). Office spaces exhibit particularly dynamic responses (**Fig. S2c**), with peak total cooling energy fluctuating between a 14.8 % reduction (July 1, 2 PM) and a 12.3 % increase (July 22, 1 PM). At night, total cooling energy in residential spaces can be saved by up to 5.2 % (July 16, 4 AM) or increased by 5.1 % (July 23, 12 AM) (**Fig. S3c**). These fluctuations highlight the dynamic interplay between microclimate modification and shading effects.

Monthly aggregated results reveal distinct net impacts by space type (Figs. 9**e** and 9**f**). For office configurations, while the 4.5 % sensible cooling savings from shading offset the 3.1 % climate-related increase, the dominant 5.3 % rise in latent demands results in a net 1.5 % cooling energy increase (Fig. 9**e**). Residential spaces present a different pattern (**Figs. S4** and **S5**), with nearly neutral sensible changes (+0.2 %) but 1.6 % higher latent demands, yielding a 0.6 % net increase (Fig. 9**f**).

These outcomes demonstrate that rooftop PV systems simultaneously create: **(1)** diurnally alternating effects with daytime sensible benefits versus nighttime penalties, **(2)** component-specific impacts where sensible loads show net reduction while latent demands exhibit net increase, and **(3)** building-type-specific performance patterns tied to operational schedules. The findings particularly emphasize that while PV shading can effectively regulate sensible loads, the microclimate changes produce more complex latent effects – increasing daytime demands but occasionally providing nighttime relief in residential settings, creating a multi-dimensional optimization challenge for PV system design that must account for building function, operational patterns, and local climate conditions.

3.5. PV capacity for peak electricity load reduction

The analysis reveals that while PV installations increase cooling demand during peak hours, they offer significant electricity generation benefits. As shown in **Fig. S6**, PV generation consistently surpasses total electricity consumption for both office and residential spaces at noon on sunny days. Fig. 10 presents the monthly averaged diurnal patterns of these effects.

For office spaces, PV installation substantially reduces net electricity consumption (total use minus generation). The system achieves 49.7 % demand reduction starting at 8 AM, with complete demand offset occurring between 12–1 PM when PV generation fully covers the floor's electricity requirements. This peak shaving capability is particularly valuable for grid management, with excess generation during the 2 PM office break period becoming available for redistribution to other floors. After 8 PM, the differences between PV-equipped and bare roofs become negligible as power generation ceases. Monthly aggregates show dramatic contrasts: PV-equipped office spaces consume just 5.59 kWh/m^2 compared to 19.25 kWh/m^2 for conventional roof, representing 71.0 % net savings (Table 4).

Residential spaces demonstrate even greater generation potential relative to daytime demand. From 11 AM to 3 PM, PV output exceeds consumption by over 100 %, creating significant surplus energy that could be utilized through energy storage systems. The net consumption

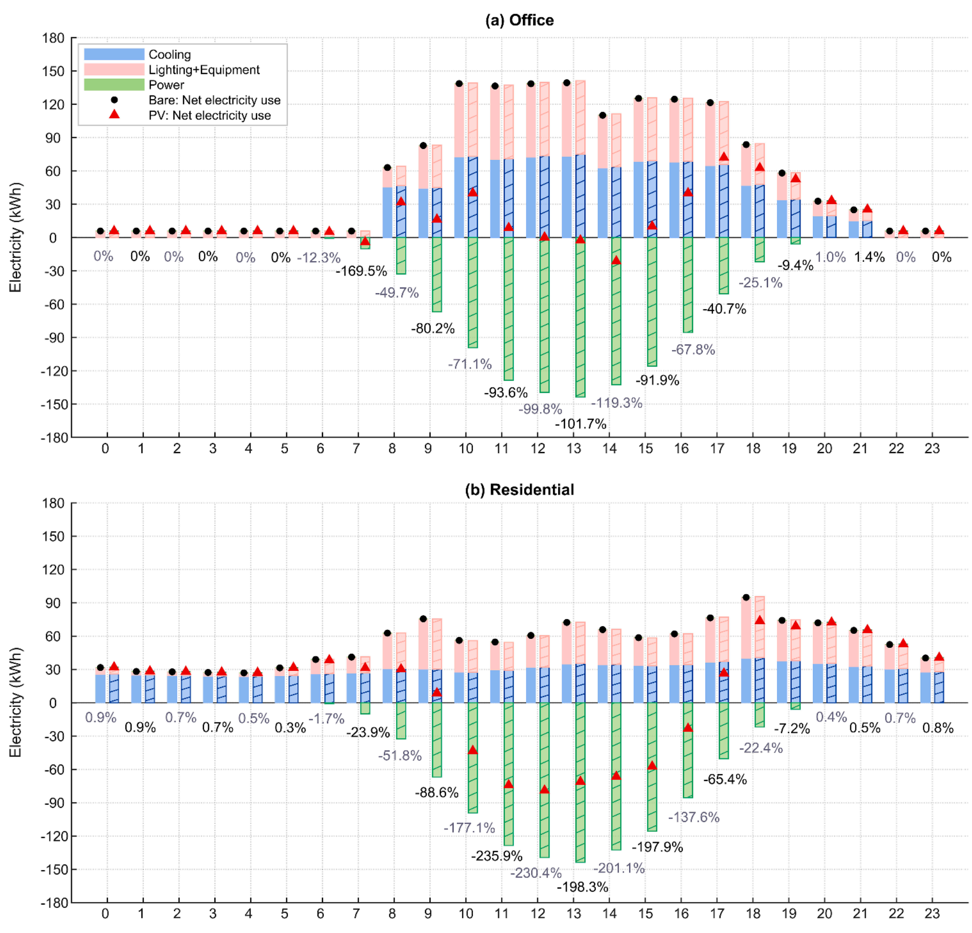

Fig. 10. Electricity generation and consumption patterns for top-floor spaces. (a) office and (b) residential configurations. Monthly averaged diurnal profiles compare bare roof (solid bars) and PV-equipped roof (shaded bars) conditions. Positive values indicate consumption; negative values represent PV power generation. Percentage values quantify the electricity savings from PV installations at each hour.

Table 4
Monthly aggregated electricity uses and power generation by scenarios, expressed in kWh per floor area (Unit: kWh/m^2).

Scenario	Cooling	Lighting+Equipment	Total	Power	Net electricity
Office setting					
Bare roof	10.15	9.10	19.25	\	19.25
PV roof	10.31	9.10	19.41	13.82	5.59
Residential setting					
Bare roof	9.73	7.61	17.34	\	17.34
PV roof	9.79	7.61	17.40	13.82	3.58

of 3.58 kWh/m² for PV-equipped residential spaces versus 17.34 kWh/m² for conventional roof (Table 4) highlights the transformative potential of PV integration, particularly when combined with storage solutions to address the temporal generation and demand mismatches.

3.6. Passive survivability assessment

Our analysis of the first week of July reveals critical insights into how rooftop PV systems affect indoor thermal conditions during power outages. As shown in Fig. 11**a**, PV installations cool outdoor air by approximately 1 °C at noon on July 1–2 compared to bare roof. However, starting from July 3, the PV site becomes hotter than the bare roof site by over 3 °C during peak heat hours.

The thermal impacts on indoor environments show more complex dynamics. Although PV shading maintains indoor temperature differences below 0.7 °C (Fig. 11**b**), it introduces substantial humidity effects that significantly affect thermal comfort. The warmer air at PV sites, despite similar outdoor RH values, contains higher absolute moisture content. This moisture-enriched air, when enters building through ventilation or infiltration, increases indoor humidity levels by up to 0.0049 kg/kg during afternoon periods (**Fig. S7**), corresponding to an 11.9 % rise in indoor relative humidity compared to control scenario (Figs. 11**c** and **S8**).

These combined thermal and humidity effects have profound consequences for heat stress indicators. On July 6, the PV-modified microclimate pushed the heat index (HI) to 65.5 °C – a dangerous 9.7 °C above control conditions (Fig. 11**d**) – and extended "Extreme Danger" exposure periods from 5 to 9 h (Fig. 11**e**). This amplification results from the heat index's nonlinear formulation (Section 2.3.4): quadratic terms (T^2, R^2)

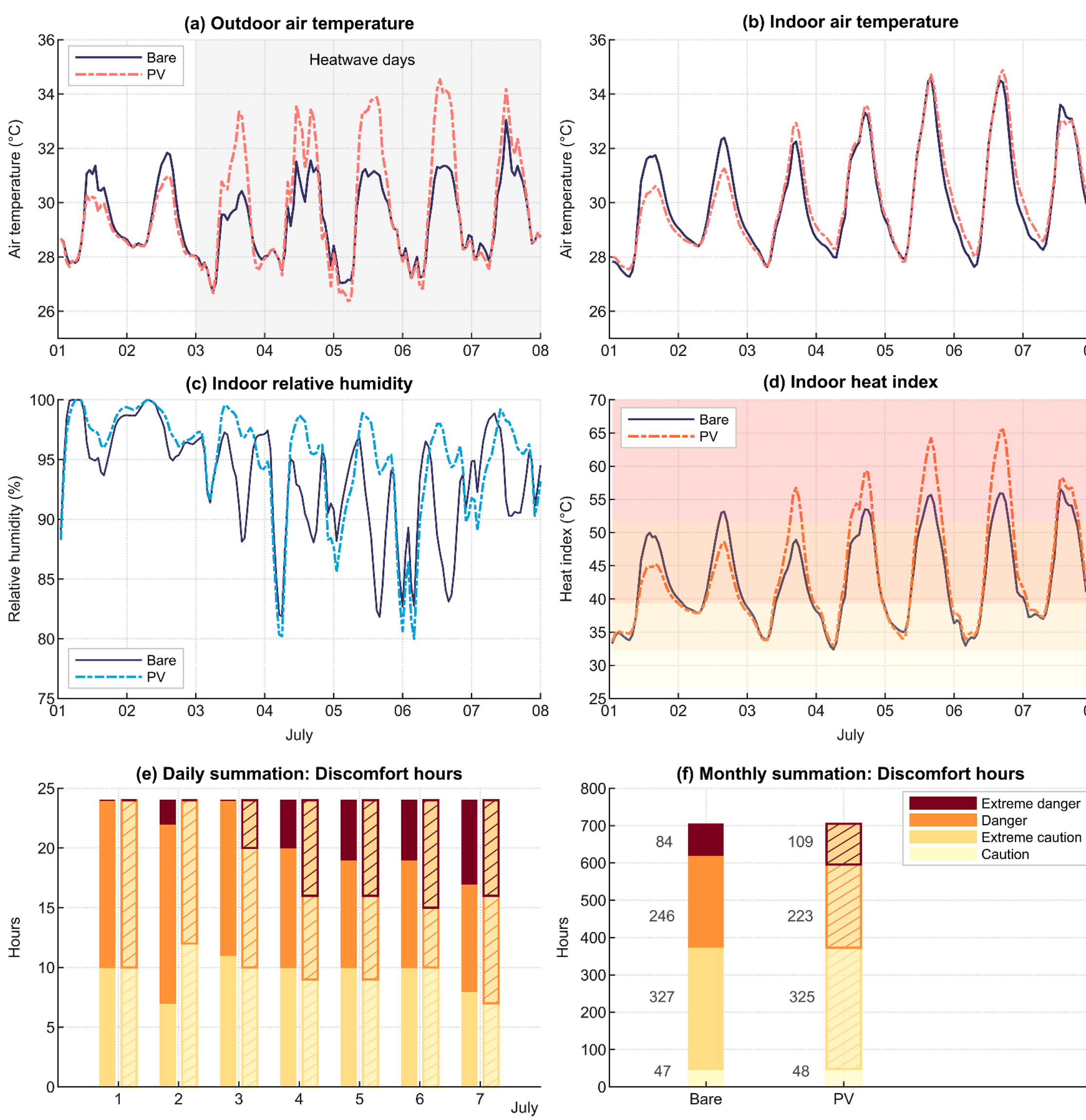

Fig. 11. Passive survivability of top-floor with and without rooftop PV. Diurnal variations of (a) outdoor air temperature, (b) indoor air temperature, (c) indoor relative humidity, (d) indoor heat index, (e) daily cumulative exposure hours by HI category (July 1–7), and (e) monthly cumulative exposure hours (July).

and interaction terms (TR, T^2R) magnify combined temperature-humidity impacts near saturation.

Monthly aggregates demonstrate that PV-equipped top-floor experiences 29.8 % more "Extreme Danger" hours (109 vs 84) while showing fewer "Danger" hours (223 vs 246) compared to conventional bare roof (Fig. 11**f**). This finding suggests that PV installations exacerbate indoor heat risks for occupants already in the "Danger" conditions, pushing them into higher risk categories.

Conventional simulation approaches using unmodified meteorological data (TMY_{Bare}) systematically underestimate heat stress risks in PV-equipped floor. As shown in Fig. 12**a**, these standard methods predict lower HI values for PV-equipped floor and identify only 64 "Extreme Danger" hours compared to the observed 109 h – a 41.3 % underestimation (Fig. 12**c**). This significant modelling gap primarily arises from neglecting PV-induced microclimate changes, particularly the increased absolute humidity in warmer PV-affected air. The discrepancy highlights that conventional assessment methods may dangerously misrepresent thermal risks, especially in hot-humid climates where humidity critically influences heat stress.

To address this challenge, these findings suggest two key mitigation strategies. **First**, thermal comfort assessments must incorporate PV-induced microclimate effects to accurately predict building performance during power outages. **Second**, we should capitalize on PV systems' inherent potential – while they may exacerbate passive heat risks through local climate modification, their electricity generation capacity could be strategically deployed to mitigate these very risks. Targeted use of PV-generated power for cooling during peak danger periods could transform these systems from passive heat amplifiers to active resilience assets, particularly valuable in climate-vulnerable regions where both energy security and thermal safety are paramount.

4. Discussions

Our findings reveal the complex interplay between rooftop photovoltaic (PV) systems and building performance through two competing mechanisms: (1) localized ambient warming primarily driven by convective heat transfer (peak ambient temperature increase of 5.2 °C), and (2) substantial rooftop cooling through shading effects (maximum surface temperature reduction of 13.4 °C). These dual effects create distinct implications for urban energy efficiency and thermal comfort management.

In humid coastal environments, PV systems demonstrate a net increase in cooling demand despite their shading benefits. While sensible cooling decreases by 1.4 % monthly due to dominant shading effect over localized warming, this gain is offset by a 4.5 % increase in latent cooling demand from higher absolute humidity, resulting in a 1.5 % net rise in total cooling consumption for office spaces. More critically, PV-induced warming extends periods of dangerous heat exposure ("Extreme Danger" conditions increased by 29.8 %), a risk underestimated by 41.3 % in conventional simulations that neglect PV-microclimate interactions. These findings highlight the need for integrated modelling approaches that account for dynamic feedback between PV systems, microclimate, and buildings in coastal environments [40,41].

Inland environments, by contrast, exhibit different behaviour due to limited moisture availability. Our supplementary analysis demonstrates that under constant absolute humidity assumptions at two roof sites, PV systems reduce midday relative humidity by up to 14.5 % due to higher air temperatures, while causing modest increases during morning and nighttime hours (up to 6.9 %) (**Fig. S9**). This leads to improved cooling performance, with monthly reductions of 1.4 % in sensible and 0.3 % in latent cooling demand for office spaces (Fig. 13**e**). Residential buildings

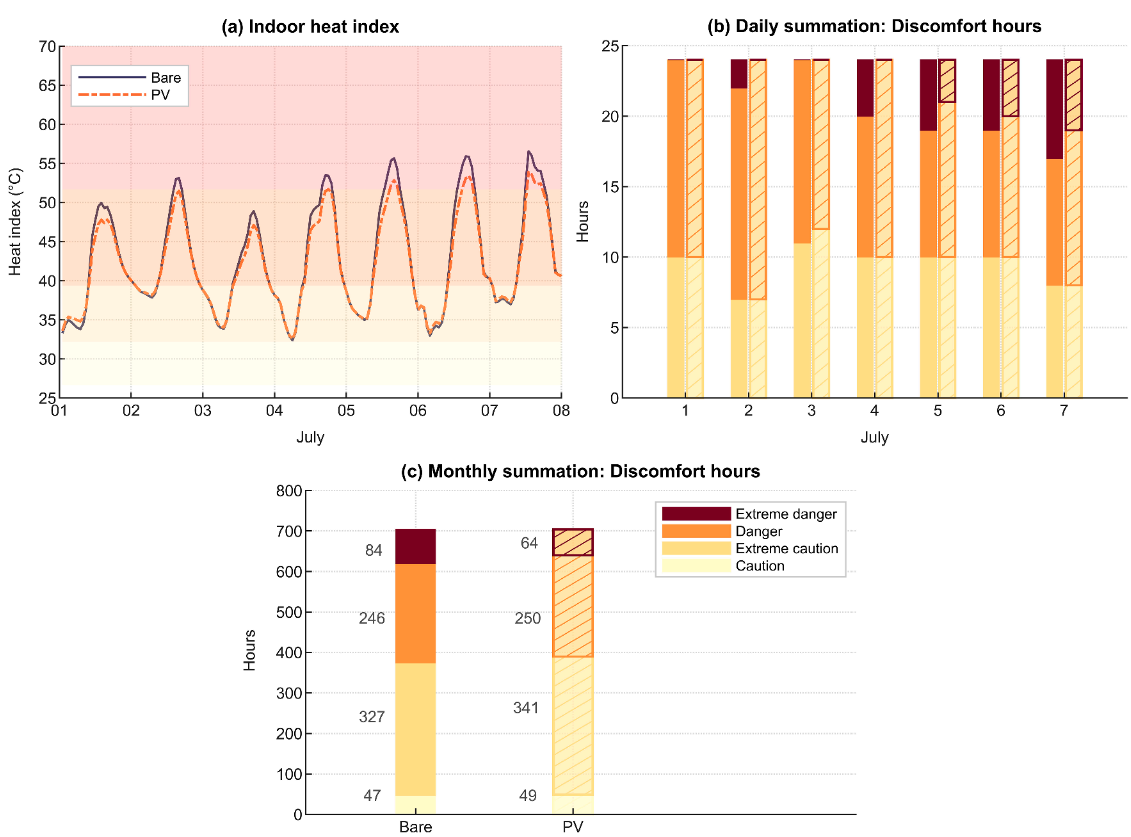

Fig. 12. Conventional simulation results of indoor heat index (HI) when neglecting PV-induced microclimate effects. (a) Diurnal variations of HI, (b) daily cumulative exposure hours by HI category (July 1–7), and (c) monthly cumulative exposure hours (July).

show similar but smaller effects (Fig. 13f). Crucially, PV installations in these regions demonstrate minimal impact on heat stress, with comparable exposure periods to “Danger” (156 vs 169 h) and “Extreme Caution” (491 vs 480 h) conditions between PV and conventional bare roofs (**Fig. S12f**). These results demonstrate that in moisture-limited environments, rooftop PV systems yield slight cooling energy savings (0.9 % for offices, 0.2 % for residences) without significantly exacerbating thermal discomfort.

These climatic contrasts highlight a critical insight: while PV temperature effects remain consistent across regions, the presence of strong humidity sources – particularly in coastal environments – dramatically alters overall system impacts. Our results therefore advocate for climate-adaptive PV deployment strategies that consider local humidity regimes. In moisture-rich coastal areas, system designs must prioritize advanced ventilation controls and enhanced dehumidification capacity to mitigate moisture-driven cooling penalties. Conversely, inland implementations can adopt more straightforward temperature-focused approaches. The excellent news is that these climate-adaptive strategies need not compromise PV’s core energy benefits – our results confirm that 50 % roof coverage still delivers 71.0 % and 79.4 % electricity savings for office and residential top-floor spaces, respectively.

Ultimately, this research establishes that **rooftop PV systems represent not just energy infrastructure, but active participants in urban microclimate systems.** Their successful integration therefore requires dual optimization: maximizing generation potential while intelligently managing localized environmental impacts. By adopting the climate-conscious design principles demonstrated here, cities worldwide can harness PV technologies to advance both energy sustainability and climate resilience. **The path forward lies not in resisting PV’s microclimate effects, but in strategically leveraging them to create smarter, more adaptive urban energy systems.**

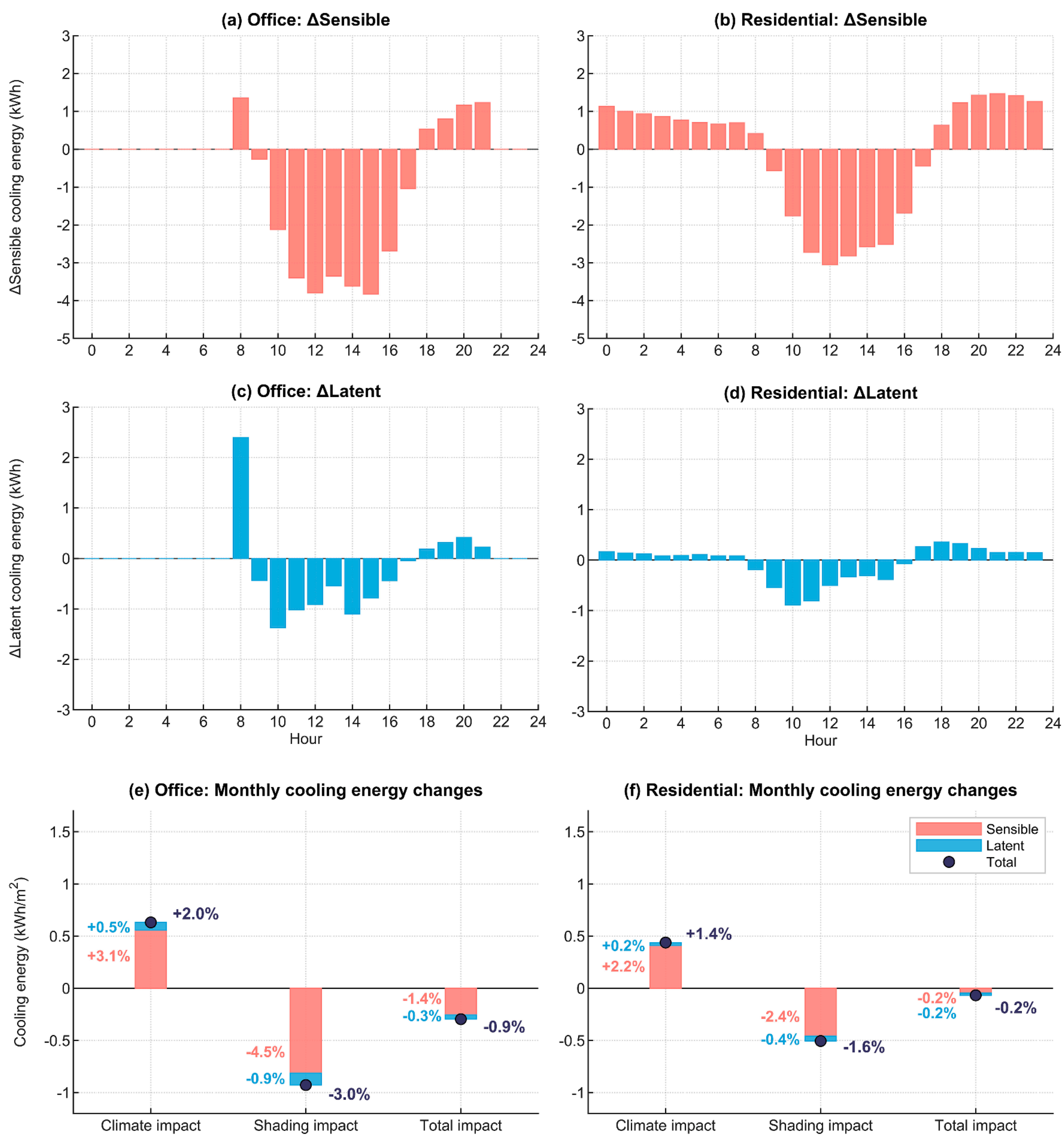

Fig. 13. Comparison of cooling energy differences between PV-equipped and control top-floor spaces, under moisture-conserved conditions. Diurnal average sensible cooling energy profile for (a) office and (b) residential use. Diurnal average latent cooling energy profile for (c) office and (d) residential use. Monthly cumulative cooling energy changes per floor area of different impacts for (e) office and (f) residential configurations.

5. Conclusions

This study demonstrates that rooftop photovoltaic (PV) systems significantly alter urban microclimates and building energy demand through two competing effects: local warming and shading. Field observations in a subtropical humid environment revealed that PV installations increased peak daytime air temperatures by up to 5.2 °C. In contrast, Energyplus simulations showed that PV shading reduced underlying roof surface temperatures by 13.4 °C. These dual mechanisms create complex energy trade-offs: shading reduced hourly sensible cooling demand by up to 14 %, but PV-induced warming increased peak sensible and latent cooling loads by 11 % and 29 % respectively during extreme heat events. At night, monthly averaged data show PV panels slightly cool ambient air (0.2 °C) but impede rooftop radiative cooling, resulting in a 2.3 % sensible cooling increase and 0.9 % latent cooling decrease at midnight. Monthly aggregates revealed a net 1.4 % sensible cooling reduction but 4.5 % latent cooling increase for office spaces, with residential spaces showing minimal net changes (0.6 % increase).

Most critically, PV-modified microclimates substantially increased heat health risks, extending "Extreme Danger" periods by 29.8 % during power outages. These findings carry important implications for urban climate adaptation, particularly in heat-vulnerable humid regions where PV systems interact strongly with nearby moisture sources. While PV generation provided substantial electricity savings (> 70 % at 50 % PV coverage), optimal integration requires designs that account for both energy production and microclimate modification to avoid exacerbating urban heat challenges.

6. Limitations and future work

While this study provides important insights into rooftop PV systems' microclimate and energy impacts, several limitations and opportunities merit discussion. The single-site field measurements should be expanded to diverse climate zones to validate these findings under different meteorological conditions, PV panel configurations (e.g., tilt angles, array spacing), and roof surface properties. Specifically, variations in PV panel thermal dissipation (affected by layout geometry and local airflow) may modify heat contribution to ambient air, while different control roof albedos (e.g., black asphalt vs. reflective membranes) establish distinct thermal baselines. Additionally, the study did not assess vertical thermal stratification around PV-equipped buildings – a gap that could be addressed through scaled experiments or urban climate modelling.

Four key research directions emerge:

First, advanced multi-scale modelling approaches could better characterize PV systems' broader climate and energy impacts. **Computational fluid dynamics (CFD)** can address panel-to-neighbourhood scale effects, where geometric parameters such as separation height and orientation angle significantly influence PV panel temperature and thermal dissipation [42,43]. The size and spacing of PV arrays affect buoyancy-induced plumes and atmospheric flow patterns [44], with thermal energy requiring 13–18 m to fully dissipate [45,46]. At larger scales, **numerical meteorological models** (e.g., WRF [16,47] and CESM [17,33]) could evaluate PV-induced modifications to urban boundary layer processes and regional/global atmospheric circulations [18,48]. Particular attention should be paid to feedback mechanisms between PV-induced cooling demand, waste heat from air conditioning systems, and urban heat island intensification (**Fig. S13**). Integrated urban climate and building energy models could enhance planning accuracy across entire districts [49–52]. Our high-resolution monitoring data from a subtropical humid site provides crucial validation benchmarks for these modelling efforts, especially valuable for coastal urban environments where observational datasets remain scarce.

Second, comprehensive assessment of human health implications is urgently needed [53]. Future work should quantify pedestrian-level thermal comfort impacts from PV-induced warm air advection, with special attention to dense urban areas where multiple PV installations may create cumulative warming effects [9,21,54]. Crucially, these assessments must consider temporal variations in heat exposure, as PV systems create distinct daytime warming and nighttime cooling patterns that affect commuters differently based on travel schedules and activity intensity. A holistic approach combining building energy, microclimate, and epidemiological methods could better characterize these health risks and inform targeted heat alert systems.

Third, innovative PV system designs should be developed and tested to mitigate adverse microclimate effects. Promising solutions include hybrid PV-green roof systems or agrivoltaics [45,55], PV integrated thermal system [56,57], reflective PV coatings [58,59], and phase-change materials [60–62]. These technologies may simultaneously reduce panel surface temperatures and improve energy conversion efficiency, helping to balance the competing priorities of renewable energy production and urban heat mitigation.

Fourth, PV deployment guidelines and building codes require revisions to address the adverse impacts. Four specific recommendations emerge: (i) Implementation of hybrid PV designs with optimized geometries to enhance passive cooling and thermal dissipation without compromising generation capacity. (ii) Establishment of minimum roof albedo standards for non-PV portions to counteract localized warming effects. (iii) Implementation of battery-backed priority circuits to ensure operation of critical cooling systems (e.g., ventilation fans) during grid outages, transforming PV systems into resilience assets during heat emergencies. (iv) Building codes in tropical humid cities (e.g., Singapore, Bangkok, Rio, and Lagos) should replace conventional dry-bulb temperature thresholds with heat index-based criteria that properly account for PV-modified humidity conditions.

Moving forward, addressing these challenges will require enhanced field measurement techniques and improved modelling approaches to better characterize PV-microclimate interactions [16,63]. These advancements will enable more accurate predictions of PV systems' role in sustainable urban development and inform effective climate adaptation strategies for cities worldwide.

CRediT authorship contribution statement

Liutao Chen: Writing – review & editing, Writing – original draft, Visualization, Methodology, Investigation, Formal analysis, Data curation, Conceptualization. **Shihong Zhang:** Software, Methodology. **Ip Cheng:** Methodology, Data curation. **Haoran Chang:** Writing – review & editing, Investigation. **Fei Chen:** Writing – review & editing, Investigation. **Mengying Li:** Writing – review & editing, Supervision, Funding acquisition. **Zhe Wang:** Supervision, Project administration, Funding acquisition.

Declaration of competing interest

The authors declare that they have no known competing financial interests or personal relationships that could have appeared to influence the work reported in this paper.

Acknowledgement

The work was supported by a grant from the Research Grants Council of the Hong Kong Special Administrative Region, China (Project No. C6003–22Y).

Supplementary materials

Supplementary material associated with this article can be found, in the online version, at doi:10.1016/j.buildenv.2025.113233.

Data availability

Data will be made available on request.

References

[1] IEA, Renewables 2023, IEA, Paris, 2024.
[2] S. Joshi, S. Mittal, P. Holloway, P.R. Shukla, B. Ó Gallachóir, J. Glynn, High resolution global spatiotemporal assessment of rooftop solar photovoltaics potential for renewable electricity generation, Nat. Commun. 12 (1) (2021) 5738.
[3] Z. Zhang, Z. Qian, M. Chen, R. Zhu, F. Zhang, T. Zhong, J. Lin, L. Ning, W. Xie, F. Creutzig, Worldwide rooftop photovoltaic electricity generation may mitigate global warming, Nat. Clim. Chang. (2025) 1–10.
[4] S. Zhang, J. Pan, B. Lin, Y. Li, M. Ji, Z. Wang, Evaluating rooftop PV's impact on power supply-demand discrepancies in grid decarbonization, Nexus 1 (4) (2024).
[5] A.H. Dehwah, M. Asif, Assessment of net energy contribution to buildings by rooftop photovoltaic systems in hot-humid climates, Renew. Energy 131 (2019) 1288–1299.
[6] V. Kapsalis, C. Maduta, N. Skandalos, M. Wang, S.S. Bhuvad, D. D'Agostino, T. Ma, U. Raj, D. Parker, J. Peng, Critical assessment of large-scale rooftop photovoltaics deployment in the global urban environment, Renew. Sust. Energy Rev. 189 (2024) 114005.
[7] D. Sailor, J. Anand, R. King, Photovoltaics in the built environment: a critical review, Energy Build. 253 (2021) 111479.
[8] Y. He, D.J.C. Hii, N.H. Wong, Solar photovoltaics deployment impact on urban temperature: review and assessment recommendations, Build. Environ. (2024) 111920.
[9] U. Berardi, J. Graham, Investigation of the impacts of microclimate on PV energy efficiency and outdoor thermal comfort, Sust. Cities Soc. 62 (2020) 102402.
[10] Q. Zhou, P. Dong, M. Li, Z. Wang, Analyzing the interactions between photovoltaic system and its ambient environment using CFD techniques: a review, Energy Build. 296 (2023) 113394.
[11] A. Cortes, Y. Murashita, T. Matsuo, A. Kondo, H. Shimadera, Y. Inoue, Numerical evaluation of the effect of photovoltaic cell installation on urban thermal environment, Sust. Cities Soc. 19 (2015) 250–258.
[12] F. Salamanca, M. Georgescu, A. Mahalov, M. Moustaoui, A. Martilli, Citywide impacts of cool roof and rooftop solar photovoltaic deployment on near-surface air temperature and cooling energy demand, Boundary Layer Meteorol. 161 (2016) 203–221.
[13] V. Masson, M. Bonhomme, J.-L. Salagnac, X. Briottet, A. Lemonsu, Solar panels reduce both global warming and urban heat island, Front. Environ. Sci. 2 (2014) 14.
[14] S. Ma, M. Goldstein, A. Pitman, N. Haghdadi, I. MacGill, Pricing the urban cooling benefits of solar panel deployment in Sydney, Australia, Sci. Rep. 7 (1) (2017) 43938.
[15] H. Taha, The potential for air-temperature impact from large-scale deployment of solar photovoltaic arrays in urban areas, Solar Energy 91 (2013) 358–367.
[16] A. Zonato, A. Martilli, E. Gutierrez, F. Chen, C. He, M. Barlage, D. Zardi, L. Giovannini, Exploring the effects of rooftop mitigation strategies on urban temperatures and energy consumption, J. Geophys. Res. Atmosph. 126 (21) (2021) e2021JD035002.
[17] A. Hu, S. Levis, G.A. Meehl, W. Han, W.M. Washington, K.W. Oleson, B.J. Van Ruijven, M. He, W.G. Strand, Impact of solar panels on global climate, Nat. Clim. Chang. 6 (3) (2016) 290–294.
[18] A. Khan, P. Anand, S. Garshasbi, R. Khatun, S. Khorat, R. Hamdi, D. Niyogi, M. Santamouris, Rooftop photovoltaic solar panels warm up and cool down cities, Nature Cities 1 (11) (2024) 780–790.
[19] W. Zhou, X. Li, L. Duanmu, C. Yuan, Investigation on rooftop PV performance and impact on microclimate in tropical cities—-A WRF modelling study in Singapore, Renew. Energy 237 (2024) 121675.
[20] B. Chen, W. Wang, Y. You, W. Zhu, Y. Dong, Y. Xu, M. Chang, X. Wang, Influence of rooftop mitigation strategies on the thermal environment in a subtropical city, Urban Climate 49 (2023) 101450.
[21] C.H. Simpson, O. Brousse, T. Taylor, J. Grellier, J. Taylor, L.E. Fleming, M. Davies, C. Heaviside, Modeled temperature, mortality impact and external benefits of cool roofs and rooftop photovoltaics in London, Nature Cities 1 (11) (2024) 751–759.
[22] L. Chen, Z. Lin, Q. Zhou, S. Zhang, M. Li, Z. Wang, Impacts of photovoltaics and integrated green roofs on urban climate: experimental insights for urban land surface modelling, Renew. Sust. Energy Rev. 217 (2025) 115709.
[23] R. Chang, Y. Shen, Y. Luo, B. Wang, Z. Yang, P. Guo, Observed surface radiation and temperature impacts from the large-scale deployment of photovoltaics in the barren area of Gonghe, China, Renew. Energy 118 (2018) 131–137.
[24] A.M. Broadbent, E.S. Krayenhoff, M. Georgescu, D.J. Sailor, The observed effects of utility-scale photovoltaics on near-surface air temperature and energy balance, J. Appl. Meteorol. Climatol. 58 (5) (2019) 989–1006.
[25] G.A. Barron-Gafford, R.L. Minor, N.A. Allen, A.D. Cronin, A.E. Brooks, M.A. Pavao-Zuckerman, The Photovoltaic Heat Island effect: larger solar power plants increase local temperatures, Sci. Rep. 6 (1) (2016) 35070.
[26] E. Fassbender, S. Pytlik, J. Rott, C. Hemmerle, Impacts of rooftop photovoltaics on the urban thermal microclimate: metrological investigations, Buildings 13 (9) (2023) 2339.
[27] E. van der Roest, J.G. Voeten, D.G. Cirkel, Increasing solar panel output with blue-green roofs in water-circular and nature inclusive urban development, Build. Environ. 244 (2023) 110704.
[28] S.S. Bhuvad, Investigation of annual performance of a building shaded by rooftop PV panels in different climate zones of India, Renew. Energy 189 (2022) 1337–1357.
[29] A. Dominguez, J. Kleissl, J.C. Luvall, Effects of solar photovoltaic panels on roof heat transfer, Solar Energy 85 (9) (2011) 2244–2255.
[30] D. Wang, T. Qi, Y. Liu, Y. Wang, J. Fan, Y. Wang, H. Du, A method for evaluating both shading and power generation effects of rooftop solar PV panels for different climate zones of China, Solar Energy 205 (2020) 432–445.
[31] V. Kapsalis, D. Karamanis, On the effect of roof added photovoltaics on building's energy demand, Energy Build. 108 (2015) 195–204.
[32] Y. He, Z. Yang, Y. Fan, Thermal performance analysis for roofs with heat mitigation strategies in subtropical hot and humid regions, Sci. Rep. 15 (1) (2025) 6117.
[33] X.C. Li, L. Zhao, Y. Qin, K. Oleson, Y. Zhang, Elevated urban energy risks due to climate-driven biophysical feedbacks, Nat. Clim. Chang. (2024) 1–8.
[34] M. Santamouris, C. Cartalis, A. Synnefa, D. Kolokotsa, On the impact of urban heat island and global warming on the power demand and electricity consumption of buildings—A review, Energy Build. 98 (2015) 119–124.
[35] Y. Kikegawa, K. Nakajima, Y. Takane, Y. Ohashi, T. Ihara, A quantification of classic but unquantified positive feedback effects in the urban-building-energy-climate system, Appl. Energy 307 (2022) 118227.
[36] H.K. Observatory, The year's weather –2024, 2025. https://www.hko.gov.hk/en/wxinfo/pastwx/2024/ywx2024.htm.
[37] R.G. Steadman, The assessment of sultriness. Part I: a temperature-humidity index based on human physiology and clothing science, J. Appl. Meteorol. Climatol. 18 (7) (1979) 861–873.
[38] Engineering Reference — EnergyPlus 9.4. https://bigladdersoftware.com/epx/docs/9-4/engineering-reference/resilience-metrics.html.
[39] NOAA, What is the heat index? https://www.weather.gov/ama/heatindex.
[40] L. Chen, J. Yang, X. Zheng, Modelling the impact of building energy consumption on urban thermal environment: the bias of the inventory approach, Urban Climate 53 (2024) 101802.
[41] T. Hong, M. Ferrando, X. Luo, F. Causone, Modeling and analysis of heat emissions from buildings to ambient air, Appl. Energy 277 (2020) 115566.
[42] M.J. Wilson, M.C. Paul, Effect of mounting geometry on convection occurring under a photovoltaic panel and the corresponding efficiency using CFD, Solar Energy 85 (10) (2011) 2540–2550.
[43] W. Gong, L. Zhang, J. Gong, X. Geng, L. Wang, L. Deng, C. Wu, E. Bao, Regulatory effect of agriphotovoltaic systems with different panel heights on the thermal environment, Sci. Rep. 15 (1) (2025) 11196.
[44] B. Stanislawski, F. Margairaz, R.B. Cal, M. Calaf, Potential of module arrangements to enhance convective cooling in solar photovoltaic arrays, Renew. Energy 157 (2020) 851–858.
[45] H.J. Williams, K. Hashad, H. Wang, K.M. Zhang, The potential for agrivoltaics to enhance solar farm cooling, Appl. Energy 332 (2023) 120478.
[46] V. Fthenakis, Y. Yu, Analysis of the potential for a heat island effect in large solar farms, in: 2013 IEEE 39th Photovoltaic Specialists Conference (PVSC), IEEE, 2013, pp. 3362–3366.
[47] F. Chen, H. Kusaka, R. Bornstein, J. Ching, C.S.B. Grimmond, S. Grossman-Clarke, T. Loridan, K.W. Manning, A. Martilli, S. Miao, The integrated WRF/urban modelling system: development, evaluation, and applications to urban environmental problems, Int. J. Climatol. 31 (2) (2011) 273–288.
[48] L. Qiu, M.F. Howland, Going beyond decarbonization: designing renewables for environmental co-benefits, Joule 8 (3) (2024) 563–565.
[49] Q. Yu, G. Ketzler, G. Mills, M. Leuchner, Exploring the integration of urban climate models and urban building energy models through shared databases: a review, Theor. Appl. Climatol. 156 (5) (2025) 266.
[50] Y. Takane, Y. Kikegawa, K. Nakajima, H. Kusaka, SLUCM+ BEM (v1. 0): a simple parameterisation for dynamic anthropogenic heat and electricity consumption in WRF-Urban (v4. 3.2), Geosci. Model Devel. 17 (23) (2024) 8639–8664.
[51] N. Sezer, H. Yoonus, D. Zhan, L.L. Wang, I.G. Hassan, M.A. Rahman, Urban microclimate and building energy models: a review of the latest progress in coupling strategies, Renew. Sust. Energy Rev. 184 (2023) 113577.
[52] S. Zhang, L. Chen, L. Xu, Z. Wang, GeoBEM: a geospatial computing empowered framework for urban-scale building energy modeling, Sust. Cities Soc. (2025) 106203.
[53] S. Wang, W. Zhan, B. Zhou, S. Tong, T. Chakraborty, Z. Wang, K. Huang, H. Du, A. Middel, J. Li, Dual impact of global urban overheating on mortality, Nat. Clim. Chang. (2025) 1–8.
[54] X. Zheng, L. Chen, J. Yang, Simulation framework for early design guidance of urban streets to improve outdoor thermal comfort and building energy efficiency in summer, Build Environ. 228 (2023) 109815.
[55] G.A. Barron-Gafford, M.A. Pavao-Zuckerman, R.L. Minor, L.F. Sutter, I. Barnett-Moreno, D.T. Blackett, M. Thompson, K. Dimond, A.K. Gerlak, G.P. Nabhan, Agrivoltaics provide mutual benefits across the food–energy–water nexus in drylands, Nat. Sust. 2 (9) (2019) 848–855.
[56] G. Asefi, A. Habibollahzade, T. Ma, E. Houshfar, R. Wang, Thermal management of building-integrated photovoltaic/thermal systems: a comprehensive review, Solar Energy 216 (2021) 188–210.
[57] A. Sohani, C. Cornaro, M.H. Shahverdian, M. Pierro, D. Moser, S. Nižetić, N. Karimi, L.K. Li, M.H. Doranehgard, Building integrated photovoltaic/thermal technologies in Middle Eastern and North African countries: current trends and future perspectives, Renew. Sust. Energy Rev. 182 (2023) 113370.
[58] M. Santamouris, Cooling the cities–a review of reflective and green roof mitigation technologies to fight heat island and improve comfort in urban environments, Solar Energy 103 (2014) 682–703.

[59] J. Yang, Z.-H. Wang, K.E. Kaloush, Environmental impacts of reflective materials: is high albedo a 'silver bullet'for mitigating urban heat island? Renew. Sust. Energy Rev. 47 (2015) 830–843.
[60] A. Scherba, D.J. Sailor, T.N. Rosenstiel, C.C. Wamser, Modeling impacts of roof reflectivity, integrated photovoltaic panels and green roof systems on sensible heat flux into the urban environment, Build Environ. 46 (12) (2011) 2542–2551.
[61] G.B. Cavadini, L.M. Cook, Green and cool roof choices integrated into rooftop solar energy modelling, Appl. Energy 296 (2021) 117082.
[62] H.M. Ali, Recent advancements in PV cooling and efficiency enhancement integrating phase change materials based systems–A comprehensive review, Solar Energy 197 (2020) 163–198.
[63] L. Chen, X. Zheng, J. Yang, J.H. Yoon, Impact of BIPV windows on building energy consumption in street canyons: model development and validation, Energy Build. 249 (2021) 111207.